Controllable red and blue bandgap energy shifted LEDs and modulators on InGaAsP quantum well platform

Parinaz Aleahmad*, Thamer Tabbakh, Demetrios Christodoulides, Patrick L. LiKamWa
CREOL/The College of Optics and Photonics, University of Central Florida, Orlando, Florida 32816, USA

ABSTRACT

Exploiting a controllable technique for red and blue shifting of quantum well's bandgap energy, we have fabricated LED sources accessing a wide frequency spectrum along with all-optical intensity modulator devices. . We demonstrate bandgap tuning of InGaAsP multiple quantum well structures by utilizing an impurity free vacancy diffusion technique. Substantial modification of the bandgap energy toward the red and blue part of the spectrum has been observed using SiO_2 , SiO_yN_x , SiN_x capping layers and by controlling the associated oxygen and nitrogen content. The resulting degree of tuning, up to 120nm red-shift and 140nm blue-shift of the band to band wavelength emission, has been studied using room temperature photoluminescence, in agreement with the emission spectra obtained from semiconductor LED devices fabricated on this platform. The intensity modulator devices has been fabricated along with LED sources compatible for the selected frequency, designed to reach minimum material losses and residual amplitude modulation.

Keywords: Bandgap tuning, quantum wells, integrated optics, on-chip modulator

1. INTRODUCTION

Photonic switches are the key components in the advance optical networks due to their great variety of applications. In this era, the InP based switches are of particular interest because of their compatibility with integration of high-performance laser diodes (LD) and light-emitting diodes (LEDs) [1-5]. This class of integrated diode lasers, open up new bandwidth regimes in telecommunication systems. Consequently, further development of these light sources will rely on the manipulations of their bandgap energy to achieve new generation of LEDs/LDs within these systems.

In this work, by utilizing a controllable technique for red and blue shifting of quantum well's bandgap energy, we have developed and fabricated LED sources monolithically integrated with broadband intensity modulator devices that are compatible with the selected spectral frequency of the LED sources. Multimode interference (MMI) geometry has been incorporated in the design of the Mach-Zehnder interferometer (MZI) modulator to control the optical intensity of the transmitted LED light. In section two, we present the simulations and design of the MMI device that operates as an integrated optical beam splitter. Section three is dedicated to the selective area disordering process that is used in order to integrate the photonic components. We demonstrate bandgap tuning of InGaAsP multiple quantum well structures by utilizing an impurity free vacancy diffusion technique. Substantial modification of the bandgap energy toward the red and blue part of the spectrum has been observed when the MQW samples are annealed using SiO_2, SiO_yN_x, or SiN_x capping layers and by controlling the associated oxygen and nitrogen content of these layers. A wide range of controllable tuning, up to 120nm red-shift and 140nm blue-shift of the optical bandgap energy of the MQWs has been achieved and measured in this section. Finally in section four, we present experimental results and fabrication process of a fully monolithically integrated device that includes an LED with a broad spectral emission and a MZI modulator with a high extinction ratio on an InGaAsP quantum well platform.

2. DESIGN AND SIMULATIONS OF MMI BASED SWITCHES AND LED

Figure 2.1 shows the schematic drawing of a monolithically integrated optical transmitter that includes a LED source and a transparent intensity modulator. The intensity modulator is based on a Mach-Zehnder interferometer (MZI) in which the phase control is achieved by injecting electrons into the core of the waveguide. The MZI is made up of two MMI couplers that serve as integrated optical beam splitters and beam combiners at the input and output of the phase modulation section. The MMI couplers as chosen in the device design owing to their compactness and tolerance to small fabrication inaccuracies, while ensuring equal optical intensities in both phase control arms of the modulator. Figure 2.2 shows the beam propagation in one such MMI device as simulated using a commercial software package (RSoft by Synopsys). In this case, it is observed that equal optical intensity division is achieved after $800\mu m$ propagation distance. The width of the MMI is set at $22\mu m$ and the center to center separation between the waveguides at the input and output is $7\mu m$.

Integrated Optics: Devices, Materials, and Technologies XX, edited by Jean-Emmanuel Broquin,
Gualtiero Nunzi Conti, Proc. of SPIE Vol. 9750, 97500N · © 2016 SPIE
CCC code: 0277-786X/16/$18 · doi: 10.1117/12.2211410

Downloaded From: http://proceedings.spiedigitallibrary.org/ on 03/06/2016 Terms of Use: http://spiedigitallibrary.org/ss/TermsOfUse.aspx

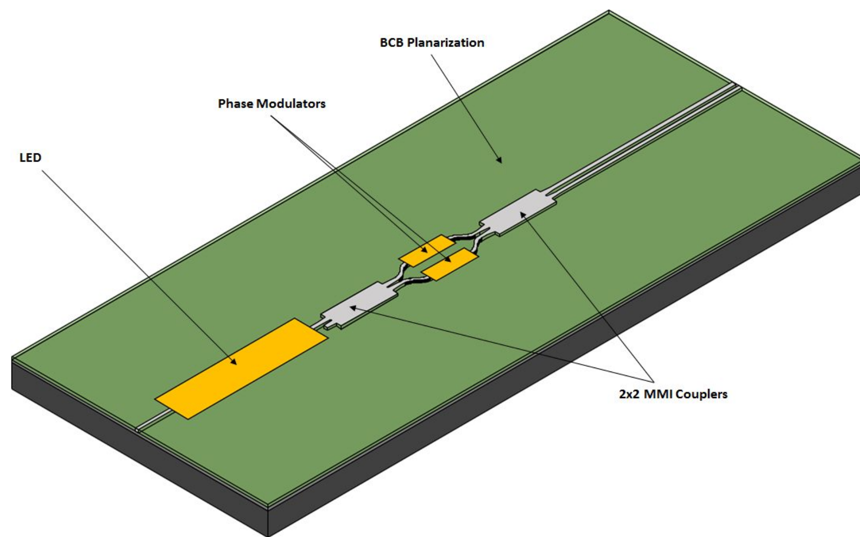

Figure 2.1. Schematic view of a completed device with monolithically integrated LED's along a MZI intensity modulator.

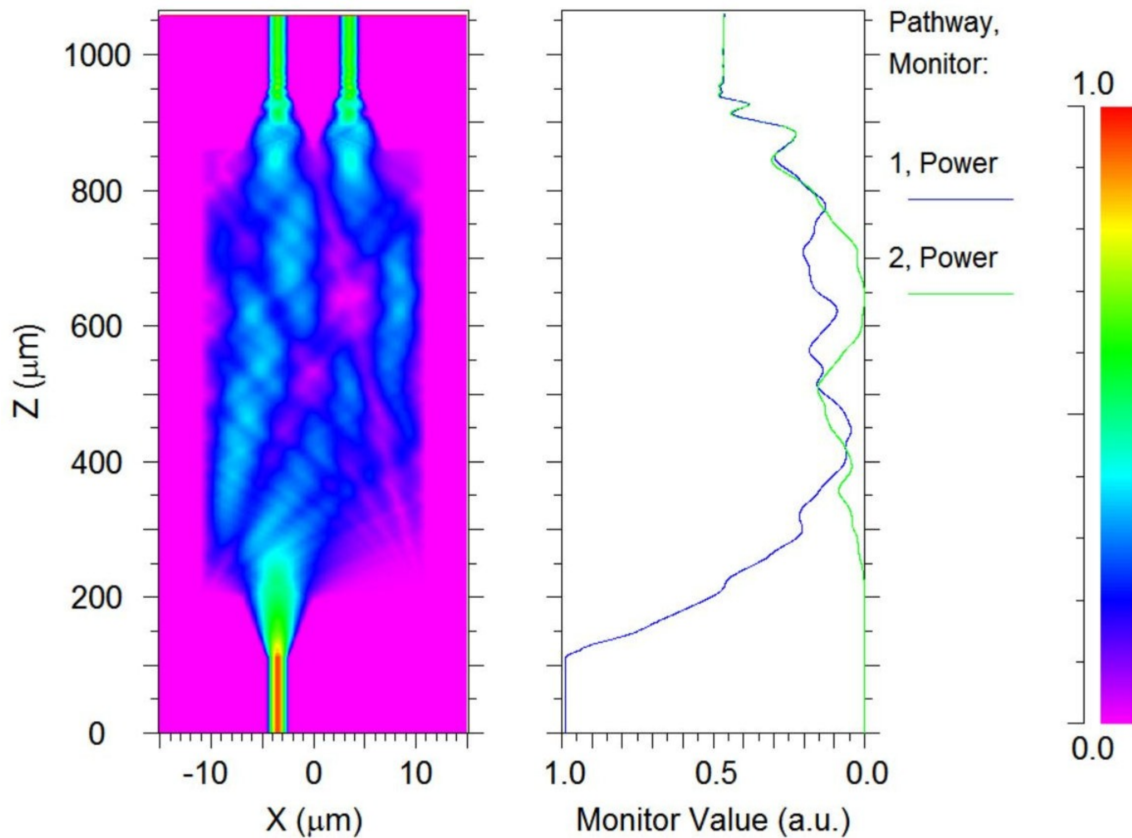

Figure 2.2. Simulation of MMI device performed by RSoft , BeamProp package. The device is designed to achieve equal optical power at the output.

Downloaded From: http://proceedings.spiedigitallibrary.org/ on 03/06/2016 Terms of Use: http://spiedigitallibrary.org/ss/TermsOfUse.aspx

3. CONTROLLABLE RED AND BLUE SHIFTING OF INGAAS QUANTUM WELL BANDGAP ENERGY

High performance semiconductor laser diodes has presented new bandwidth regimes in optical communications. However the frequency of such optical sources are yet restrained by the band structure of its contrived quantum well platforms. Thus, retaining control over the frequency domain of such structures can be of great interest in these systems as it will offer a wide range of new optical sources. Selective bandgap tuning of quantum wells has been an ongoing task in recent years [6-22]. The objective in these recent studies is mostly focused on reducing the optical losses by blue shifting the original bandgap energy. In this work however we present a controllable red and blue shifting of the band to band wavelength emission up to 120nm toward red and 140nm toward blue. Among the many techniques that has been utilized for this purpose, induced disordering of MQWs by impurity-free vacancy diffusion (IFVD) attracted a great deal of attention due to its ability to conserve the electrical properties of the quantum well structure and its good selectivity in the spatial domain. The IFVD techniques are usually performed by selecting a capping layer, SiO_2 in the case of group InGaAsP materials, which promotes the out-diffusion of Ga atoms from the top layer of the semiconductor into the upper dielectric capping layer through a rapid thermal annealing. As the annealing continues, the vacancies that are thus introduced at the surface, rapidly migrates towards the substrate layer. As the vacancies pass through the MQW layers, they exchange lattice sites with constituent atoms of the well and barrier materials causing a significant inter-diffusion of the species especially at the well/barrier interfaces. The SiO_2 film therefore usually causes the bandgap of the quantum wells to increase (blue shifting of the absorption edge). Covering the surface of the semiconductor with SiN_x usually serves to prevent the out-diffusion of Ga atoms from the top surface, thereby protecting the MQW below from intermixing [15, 16, 19]. The dielectric film properties and the annealing condition in this technique play a critical role in the degree of intermixing. In addition to this parameters, we showed that, the manipulation of the Nitrogen and Oxygen shares in the top cladding films can bring a wide range of selectivity for the blue/red shifting of the bandgap energies. To confirm the mentioned tunings, we collect the photoluminescence spectra of the disordered samples along with the emission spectra of LED devices fabricated on the disordered quantum well wafers which corroborate with the former photoluminescence measurements.

The structure used as the platform in this study consists of six InGaAsP quantum wells grown by metal organic chemical vapor deposition (MOCVD) at a commercial semiconductor foundry. The p-i-n structure is grown epitaxially on a Si doped InP substrate with a 70nm thick undoped InGaAsP buffer at the n-i and p-i interface. The active region consists of six undoped InGaAsP ($\lambda_g = 1.56\ \mu m$) quantum wells each 8nm thick sandwiched between five undoped layers of 15nm thick InGaAsP ($\lambda_g = 1.13\ \mu m$) barriers, where λ_g is the bandgap wavelength. The wafer design is shown in figure 3.1.

Layer	Thickness
InGaAs p-type	100nm
InP p-type (Zn dopped)	1000nm
InGaAsP U/D	70nm
5×InGaAsP (15nm)/6×InGaAsP(8nm)	
InGaAsP U/D	70nm
InP n-type (Si dopped)	2500nm
InGaAs n-type (Si dopped)	50nm
InP Substrate (Si dopped)	

Figure 3.1. Schematic cross sectional view of MQW grown by MOCVD.

Downloaded From: http://proceedings.spiedigitallibrary.org/ on 03/06/2016 Terms of Use: http://spiedigitallibrary.org/ss/TermsOfUse.aspx

Several samples have been prepared with a variety of SiO_2, SiN_x and SiO_yN_x films grown by plasma-enhanced chemical vapor deposition (PECVD) as the capping layers. Table 3.1 shows the different recipes that were used to grow the variety of films. In the evaluation process, the top surface of each sample was first covered by a film of a SiN_x or SiO_yN_x using PECVD. Then half of the surface film was removed by the reactive-ion etching (RIE) process and a 200nm thick film of SiO_2 was grown by PECVD, on the whole surface. As indicated in table 3.1, the different SiO_yN_x films were generated by manipulation of the ratio of N_2O to NH_3 to control the eventual content of oxygen in the dielectric film. It is fair to assume that a larger oxygen content will lead to a lower refractive index whereas a larger nitrogen content will lead to a higher refractive index. Furthermore, another set of SiN_x films was generated in the absolute absence of N_2O, where the only controllable parameter was the silicon to nitrogen ratio which was achieved by varying the SiH_4 to NH_3 ratio during the PECVD growth. Here a silicon rich SiN_x film will exhibit a higher refractive index. However in the final analysis, to be able to compare all the dielectric films together, we have sorted them according to their refractive indices. The thickness of the SiN_x/SiO_yN_x films was kept at 30nm as a good compromise between repeatability and film robustness to high temperature anneals. Each sample then was treated individually in a rapid thermal annealer (RTA) for 30 sec at 800^oC.

The absolute values of photoluminescence (PL) peak shift from that of the as-grown sample is plotted in figure 3.2 as a function of the refractive indices of the covering films. The down-pointing triangles indicate SiO_yN_x films while the up-pointing triangles refers to SiN_x claddings. From this figure, an absolute shift of bandgap energy equal to -140nm toward blue and +120nm toward red is recognizable. As expected, the SiO_yN_x films with higher share of Oxygen tends to bring a blue shift similar to the SiO_2 films, while larger ratios of NH_3/N_2O produce SiO_yN_x films that contain larger x/y ratios with correspondingly higher refractive indices tend to shift the PL to a longer wavelength. However in the absence of N_2O component, the SiN_x films lead to red shifting of the PL peak. The degree of this red-shift could be controlled by the ratio of SiH_4 to NH_3, with a larger ratio of SiH_4/NH_3 resulting in more bandgap narrowing of the MQWs.

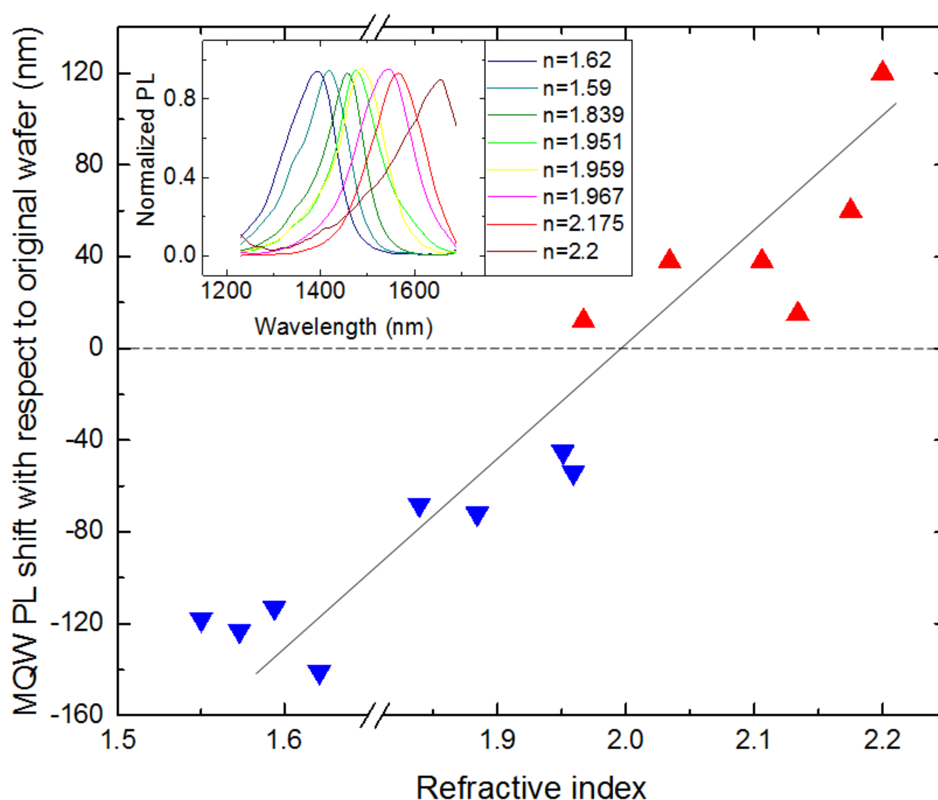

Figure 3.2. Measured absolute value of the PL shift of the RTA treated samples from that of the as-grown wafer for different dielectric film capping, in respect to the refractive index of the film. The blue shift associated with SiO_yN_x films for different ratios of NH_3/N_2O, while the red shift refers Si-rich compositions. The inset shows the absolute PL spectrum for selected data points.

Downloaded From: http://proceedings.spiedigitallibrary.org/ on 03/06/2016 Terms of Use: http://spiedigitallibrary.org/ss/TermsOfUse.aspx

	Power(W)	Temp(oC)	SiH_4(sccm)	NH_3(sccm)	N_2O(sccm)	N_2(sccm)	HE(sccm)	Index of Refraction
1	150	300	200	4	20	800	0	1.55
2	100	250	200	10	35	600	0	1.573
3	100	250	200	10	29	600	0	1.594
4	150	300	180	3.5	10	800	0	1.621
5	150	300	180	3.5	5	800	0	1.839
6	100	250	180	4.2	0	200	219	1.884
7	150	300	180	4	0	0	450	1.951
8	150	300	200	4	4	800	0	1.959
9	100	250	240	4	0	200	219	1.967
10	150	300	180	4.2	0	200	219	2.034
11	150	300	180	3.75	0	200	219	2.106
12	150	300	200	4	0	800	0	2.134
13	150	300	220	4	0	200	219	2.175
14	150	300	200	3.5	0	800	0	2.2

Table 3.1. Recipes for SiN/ SiO_yN_x film composition sorted with respect to their refractive index;

A more thorough study has been focused on SiN_x films of varying Si compositions. To reduce any other unintended influences, in the growth of the SiN_x films, the SiH_4, He and N_2 mass flow rates as well as the plasma RF power and the substrate temperature were all kept constant while changing the NH_3 flow for all different recipes. Figure 3.3 shows the absolute PL shift of such samples treated with RTA. The results clearly show a red shifting of the PL peak emission for Si-rich compositions of SiN_x with the largest shift occurring when the ratio of SiH_4 to NH_3 is highest during the PECVD process.

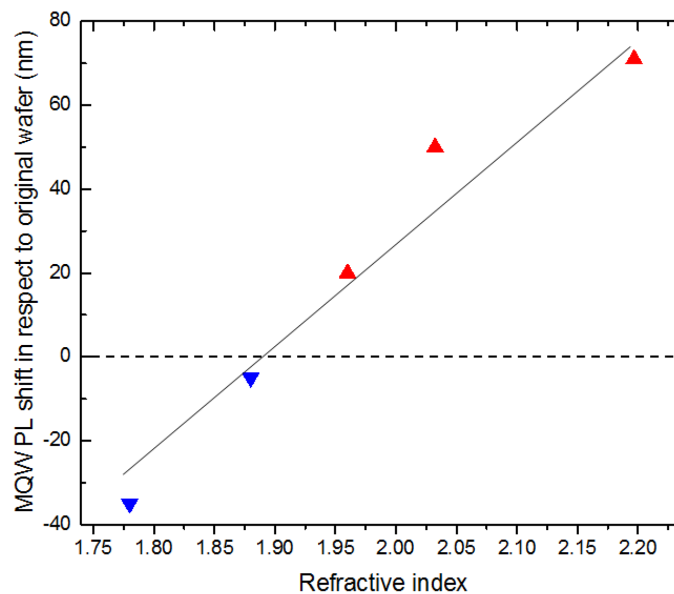

Figure 3.3. Blue/Red shifting of PL emission peak from a MQW structure disordered by different SiN_x films.

Downloaded From: http://proceedings.spiedigitallibrary.org/ on 03/06/2016 Terms of Use: http://spiedigitallibrary.org/ss/TermsOfUse.aspx

4. DEVICE FABRICATION AND MEASUREMENTS

4.1 Fabrication

The samples used in this study were ultrasonically cleaned with acetone, followed by rinsing with isopropyl alcohol (IPA) and deionized (DI) water to remove debris and organic residue from the exposed surfaces. The samples were then immersed in buffered oxide etch (BOE) to remove any native oxide from the surface. In this experiment, a 30nm thick film of SiN_x film was deposited by PECVD on the top layer. The regions of the MQW that needed to be protected from disordering were delineated using photoresist and photolithography. The other parts of the SiN_x is removed by RIE. After cleaning off the photoresist, a 200nm thick film of SiO_2 was deposited over the whole surface for the purpose of intermixing the regions of the semiconductor in contact with the SiO_2 film. The samples were then annealed at 775°C for 30 seconds in a nitrogen atmosphere. The sample with selected regions that have been disordered, and still covered by the SiN_x and SiO_2 films, was then coated with photoresist. The device structures were then photolithographically patterned into the photoresist. These patterns were then transferred into the SiN_x and SiO_2 films by RIE and then the uncovered regions of the top InGaAs layer were removed using a mixture of H_3PO_4:H_2O_2:H_2O in a volume ratio of 1:1:30 respectively. The unwanted InP layer was then etched off using a 1:1 mixture of HCl:H_3PO_4. After all the waveguide structures have been delineated, the originally deposited SiN_x and SiO_2 films were then removed completely using RIE. The top surface was planarized by spin-coating the sample with benzocyclobutene (BCB) resin (commercially known as Cyclotene), and etching it off until only about 200nm of the top InGaAs layer was exposed. P-type contact metals consisting of Ti, Zn and Au were then deposited on top of the waveguides that operate as LEDs and phase modulation sections. The sample was annealed at 430ºC for 30s to improve the adhesion of the metal contacts to the surface of the semiconductor. Figure 4.1 shows microscope photographs of the fabricated device after the metal deposition from top view. The sample was then lapped and polished to a final thickness of 120nm before the n-type contact metals (Ni, Ge, Au) were deposited on the substrate side of the devices. The sample was cleaved to an overall length of 6.5mm and mounted on a temperature controlled heat-sink.

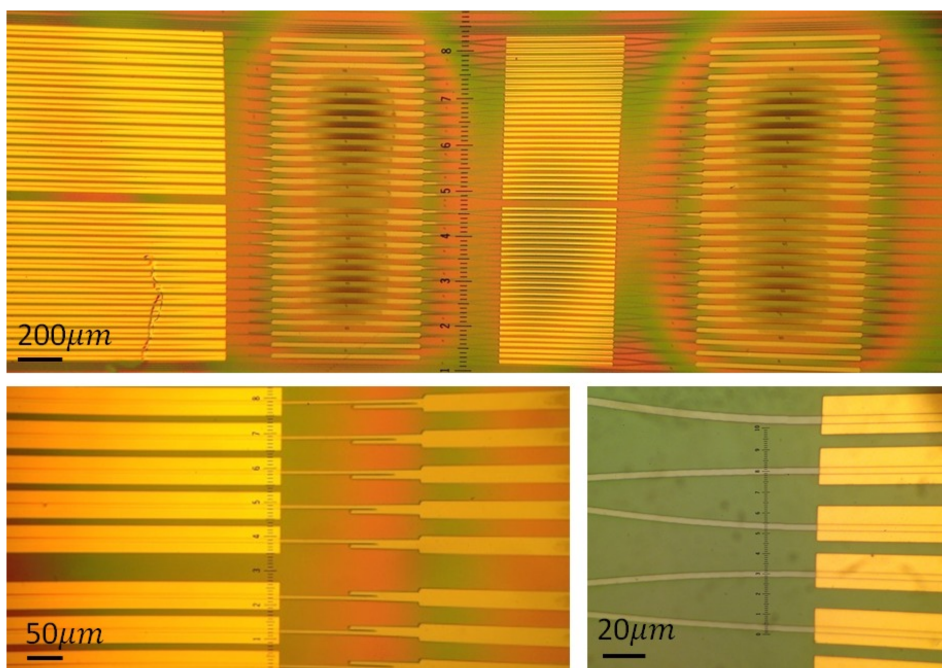

Figure 4.1. Fabricated device containing two sets of MMI, and LEC source and a MZI in between. The scales has been changed for clarification for the device.

4.2 LED devices

In the regions of the sample where the MQWs were covered by SiN_x film during the rapid thermal annealing, and consequently were not disordered, the ridge waveguides with electrical contacts on top conveniently form edge emitting

Downloaded From: http://proceedings.spiedigitallibrary.org/ on 03/06/2016 Terms of Use: http://spiedigitallibrary.org/ss/TermsOfUse.aspx

p-i-n LEDs. The I-V characteristics of the LEDs exhibit clear diode behavior with about 5mA flowing with a 1V forward bias whereas it appears as an open-circuit when driven in reverse bias with the current driver. The light output from the LED waveguide was captured by a lens and directed to a power meter. Figure 4.2 shows the light vs current (L-I) response of one such LED as well as its emission spectrum which is centered at 1547nm.

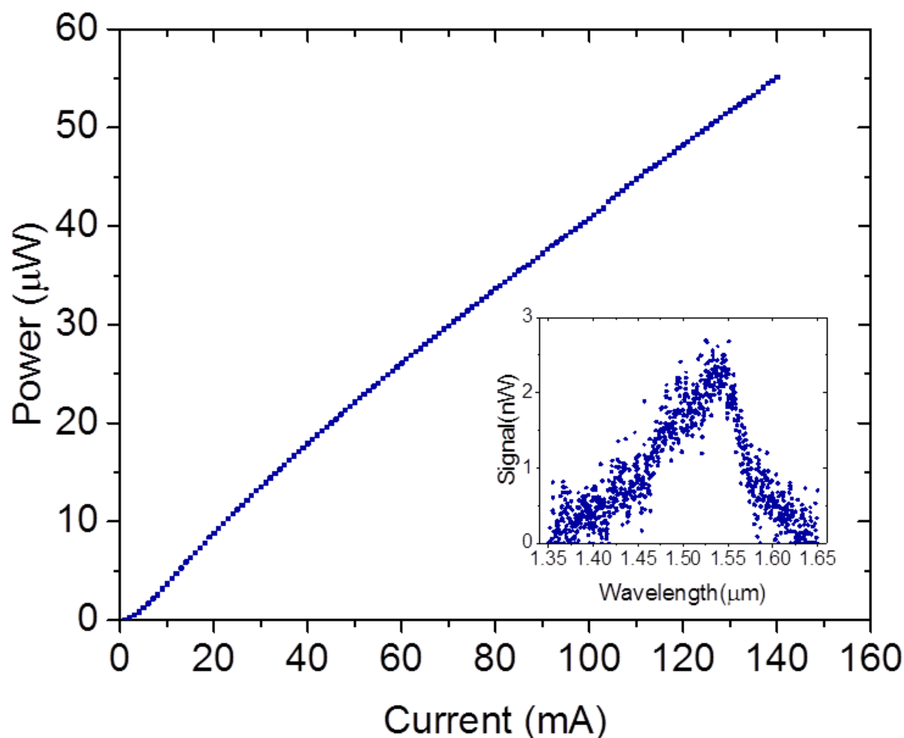

Figure 4.2. The L-I curve one of the LED devices. The inset shows the spectrum of the LED at a current of 100mA .

4.3 Integrated LED transmitter measurements

The fully integrated devices were tested by first energizing the LED with a constant 135mA injection current. The light output from the two output waveguides of the MZI were imaged simultaneously on an infrared camera and a p-i-n photodiode using a X20 microscope objective lens. An adjustable slit on a translation stage was placed in front of the photodiode so that it can measure the output power from either port independently. Electrical current from a second current driver was injected into one of arms of the MZI. Figure 4.3 shows the captured images of the output ports as the current was varied.

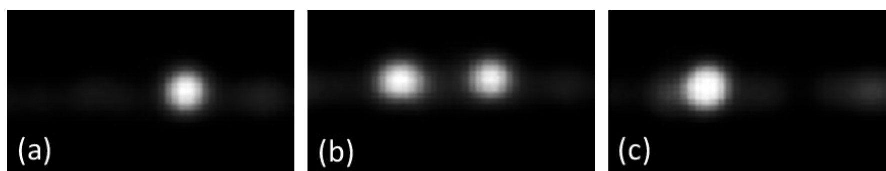

Figure 4.3. Optical power distribution of MZI's two output channel at a) I=0mA, b) I=0.67mA and c)1.47mA.

The output power from each of the two waveguides after the second MMI were then recorded as a function of the current passing through the MZI device. Figure 4.4 shows the normalized value of optical power from each output channel with respect to the injected current for two full switching cycles.

As current was injected into the phase control waveguide, it was observed that optical power was being transferred from the right output port into the left output port. Until at about 0.67 mA injected into the waveguide, the optical power was

Downloaded From: http://proceedings.spiedigitallibrary.org/ on 03/06/2016 Terms of Use: http://spiedigitallibrary.org/ss/TermsOfUse.aspx

almost equally divided between the two output waveguides. With 1.47mA injected into the waveguide, all of the optical power was switched to the left output port. Figure 4.4 shows the switching characteristics of the integrated MZI modulator. It is evident that the current needed to achieve a π-phase shift in one arm of the interferometer is only 1.47mA. However, the measurements also indicated that beyond that current level, the phase modulation was no longer pure and there was an onset of current induced intensity change in one arm of the interferometer leading to incomplete interferometric cancellation at the second MMI. This resulted in a diminished extinction ratio at the second switching half-cycle. Furthermore, the second switching current occurred at 4.7mA which was significantly larger than double the switching current for the first half-cycle, indicating an onset of saturation of the electron density induced refractive index change.

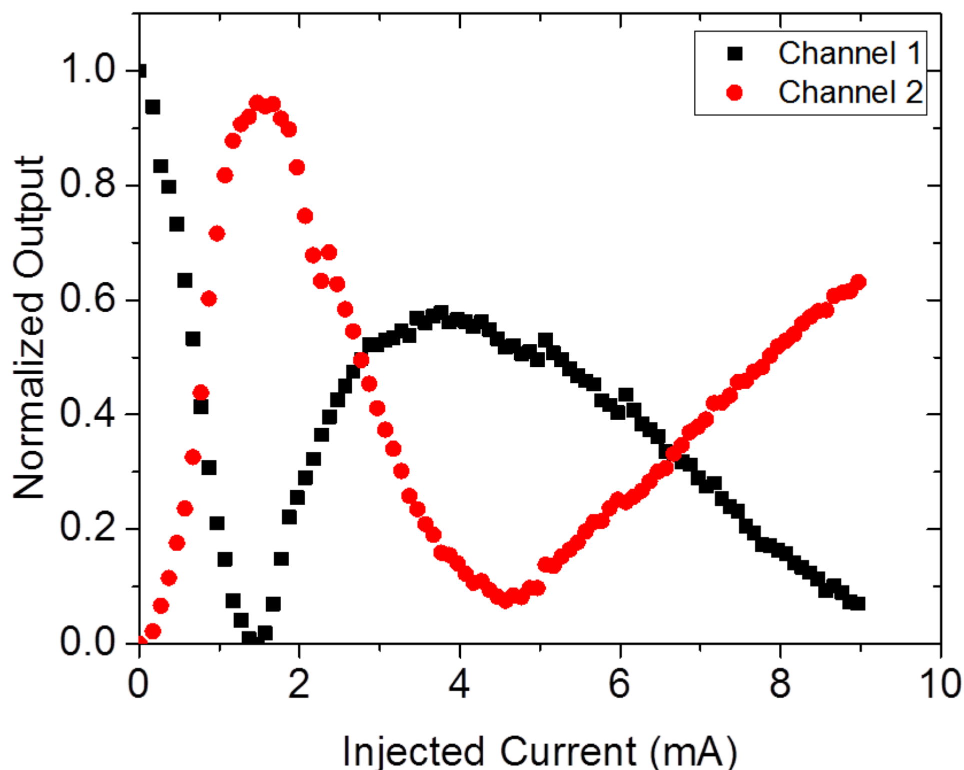

Figure 4.4. Measured optical power at the output of each port as a function of the injected current.

5. CONCLUSION

In conclusion, we have developed a method of area selectively disordering MQWs for the purpose of fabricating active monolithically integrated optoelectronic circuits. In this work, we report the fabrication of an integrated LED transmitter composed of a broadband LED source and an inline MZI modulator with two MMI couplers/splitters. The optical transmitter with a spectral bandwidth of about 100nm (FWHM) operates at a switching current of 1.47mA.

Downloaded From: http://proceedings.spiedigitallibrary.org/ on 03/06/2016 Terms of Use: http://spiedigitallibrary.org/ss/TermsOfUse.aspx

REFERENCES

1. Yu, S.F. and E.H. Li, *Semiconductor lasers using diffused quantum-well structures.* Ieee Journal of Selected Topics in Quantum Electronics, 1998. **4**(4): p. 723-735.
2. Kim, C., et al., *Ultrafast all-optical multiple quantum well integrated optic switch.* Electronics Letters, 2000. **36**(23): p. 1929-1930.
3. Choy, W.C.H. and K.S. Chan, *Theoretical analysis of diffused quantum-well lasers and optical amplifiers.* Ieee Journal of Selected Topics in Quantum Electronics, 2003. **9**(3): p. 698-707.
4. Taniguchi, H., et al., *25-W 915-nm lasers with window structure fabricated by impurity-free vacancy disordering (IFVD).* Ieee Journal of Selected Topics in Quantum Electronics, 2007. **13**(5): p. 1176-1179.
5. Zhao, J., et al., *Spatial control based quantum well intermixing in InP/InGaAsP structures using ICP.* Journal of Semiconductors, 2012. **33**(10): p. 106001.
6. Rao, S., W. Gillin, and K. Homewood, *Interdiffusion of the group-III sublattice in In-Ga-As-P/In-Ga-As-P and In-Ga-As/In-Ga-As heterostructures.* Physical Review B, 1994. **50**(11): p. 8071-8073.
7. Rao, E.V.K., et al., *New encapsulant source for III–V quantum well disordering.* Applied Physics Letters, 1995. **66**(4): p. 472.
8. Pepin, A., et al., *Evidence of stress dependence in SiO2/Si3N4 encapsulation-based layer disordering of GaAs/AlGaAs quantum well heterostructures.* Journal of Vacuum Science & Technology B, 1997. **15**(1): p. 142-153.
9. Choi, J., et al., *Dependence of dielectric-cap quantum-well disordering of GaAs-AlGaAs quantum-well structure on the hydrogen content in SiN/sub x/ capping layer.* IEEE Journal of Selected Topics in Quantum Electronics, 1998. **4**(4): p. 624-628.
10. Kowalski, O.P., et al., *A universal damage induced technique for quantum well intermixing.* Applied Physics Letters, 1998. **72**(5): p. 581.
11. Sang Kee, S., et al., *Area selectivity of InGaAsP-InP multiquantum-well intermixing by impurity-free vacancy diffusion.* IEEE Journal of Selected Topics in Quantum Electronics, 1998. **4**(4): p. 619-623.
12. Helmy, A.S., et al., *Control of silica cap properties by oxygen plasma treatment for single-cap selective impurity free vacancy disordering.* Applied Physics Letters, 1999. **74**(5): p. 732-734.
13. Liu, X.F., et al., *Control of multiple bandgap shifts in InGaAs-AlInGaAs multiple-quantum-well material using different thicknesses of PECVD SiO₂ protection layers.* IEEE Photonics Technology Letters, 2000. **12**(9): p. 1141-1143.
14. Lee, A.S.W., et al., *Enhanced band-gap blueshift due to group V intermixing in InGaAsP multiple quantum well laser structures induced by low temperature grown InP.* Applied Physics Letters, 2001. **78**(21): p. 3199.
15. Teng, J.H., et al., *Controlled group V intermixing in InGaAsP quantum well structures and its application to the fabrication of two section tunable lasers.* Journal of Applied Physics, 2002. **92**(8): p. 4330.
16. Choi, W.J., et al., *Dependence of the intermixing in InGaAs/InGaAsP quantum well on capping layers.* Journal of the Korean Physical Society, 2004. **45**(3): p. 773-776.
17. Skogen, E.J., et al., *Multiple-band-edge quantum-well intermixing in the InGaAs/InGaAsP/InGaP material system.* Applied Physics Letters, 2005. **86**(24): p. 241117.
18. Helmy, A.S., et al., *Spatially resolved photoluminescence and Raman spectroscopy of bandgap gratings fabricated in GaAs/AlAs superlattice waveguide using quantum well intermixing.* Journal of Crystal Growth, 2006. **288**(1): p. 53-56.
19. Yu, J.S. and Y.T. Lee, *Impurity-free vacancy diffusion of InGaAsP/InGaAsP multiple quantum well structures using SiH4-dependent dielectric cappings.* Japanese Journal of Applied Physics Part 1-Regular Papers Brief Communications & Review Papers, 2007. **46**(10A): p. 6509-6513.
20. May-Arrioja, D.A., et al., *Intermixing of InP-based multiple quantum wells for integrated optoelectronic devices.* Microelectronics Journal, 2009. **40**(3): p. 574-576.
21. McKerracher, I., et al., *Intermixing of InGaAs/GaAs quantum wells and quantum dots using sputter-deposited silicon oxynitride capping layers.* Journal of Applied Physics, 2012. **112**(11): p. 113511.
22. Bickel, N. and P. LikamWa, *Enhanced control over selective-area intermixing of In0.15Ga0.85As/GaAs quantum dots through post-growth exposure to radio-frequency plasma.* Thin Solid Films, 2011. **519**(6): p. 1955-1959.

Downloaded From: http://proceedings.spiedigitallibrary.org/ on 03/06/2016 Terms of Use: http://spiedigitallibrary.org/ss/TermsOfUse.aspx